JOURNAL OF THERMOPHYSICS AND HEAT TRANSFER
Vol. 22, No. 2, April–June 2008

Temperature Range and Conjugate Effects in Microencapsulated Phase-Change Suspensions

Daniel Cassidy* and Richard D. Gould†
North Carolina State University, Raleigh, North Carolina 27695

DOI: 10.2514/1.33560

The melting process of some phase-change materials does not occur at a single temperature, but rather occurs over a temperature range. The effect of a phase-change temperature range for microencapsulated phase-change-material slurry was investigated numerically for a hydrodynamically fully developed laminar flow in a circular tube with a constant wall heat flux. The wall temperature and exit radial temperature were investigated for several phase-change temperature ranges, including a single phase-change temperature. The dominant dimensionless parameters: Stefan number, melt temperature range, and subcooling were varied and results presented. For code verification, results were compared with previous experimental and numerical data using eicosane as the phase-change material. Using heat flow measurements over the melt region from current literature, a curve fit for eicosane was made and used in the numerical model. The numerical results compared well with existing experimental and numerical findings and showed the phase-change region was the cause of temperature discrepancies cited in previous numerical work.

Nomenclature

B, m	=	constants
Bi	=	Biot number, h/k
C	=	specific heat, J/kg · K
c	=	volumetric concentration of particles
e	=	velocity gradient, 1/s, du/dr
F	=	mass fraction
f	=	specific heat function, J/kg · K
H	=	enthalpy, J/kg
h	=	heat transfer coefficient, W/m^2 · K
K	=	thermal conductivity ratio, k_f/k_w
k	=	thermal conductivity, W/m · K
L	=	latent heat, J/kg
Nu	=	Nusselt number, $h2R/k$
Pr	=	Prandtl number, ν/α
q''	=	heat flux, W/m^2
R	=	tube outside diameter, m
Re	=	Reynolds number, $u_m 2R/\nu$
r	=	radial coordinate, m
S	=	source term
Ste	=	Stefan number, $(C_b q''_R R/k_b)/(cL\rho_p/\rho_b)$
T	=	temperature, °C
U	=	overall heat transfer coefficient, W/m^2 · K
u	=	axial velocity, m/s
z	=	axial coordinate, m
$\propto$	=	viscosity, m^2/s
Δ	=	dimensionless tube wall thickness, δ/R
δ	=	tube wall thickness
ε	=	fraction of latent heat (0–1)
θ	=	dimensionless temperature, $(T - T_{\text{in}})/(q''R/k_b)$
ρ	=	density, kg/m^3
σ	=	standard deviation
τ	=	integration place holder

Subscripts

app	=	apparent
b	=	bulk fluid
e	=	exit
eff	=	effective
f	=	fluid
l	=	liquid
m	=	mean
p	=	particle
R	=	inside tube radius
s	=	solid
sb	=	subcooling
sl	=	solid to liquid
w	=	wall
0	=	inlet

Superscripts

$*$	=	dimensionless variable
$+$	=	alternate definition

Introduction

ENHANCED heat transfer characteristics are found when a phase-change material (PCM) is microencapsulated and added to a heat transfer liquid in a heat exchange system. Typical carrier fluids include antifreeze, water, silicon oil, etc., and the microPCM is typically paraffin. The resulting two phase system is able to absorb larger amounts of heat over a temperature range, which includes the phase-change temperature. The increase of thermal storage is due to latent heat storage occurring as the microencapsulated PCM changes from a solid phase to a liquid. Such fluids have potential as pumped loop cooling media for applications in aerospace electronics cooling, terrestrial energy systems, and recently in electric vehicle cooling [1] and microchannels [2].

Over the years there have been numerical and experimental studies of the heat transfer in circular tubes using a microPCM slurry [3–6]. Charunyakorn et al. [3] performed a numerical simulation of slurry in a circular duct, which was then followed by the experimental work of Goel et al. [4] for the same fluid PCM combination. There was a large discrepancy between the numerical predictions and experimental findings. Several possible sources of these discrepancies were attributed to physics not included in the numerical method and were listed by Goel et al. [4]. These included a phase-change temperature range instead of a single melt temperature, assuming the entire particle consisted of the PCM, increased thermal resistance between

Received 18 July 2007; revision received 16 January 2008; accepted for publication 20 January 2008.

*Graduate Student, Department of Mechanical and Aerospace Engineering, Campus Box 7910.

†Professor and Department Head, Department of Mechanical and Aerospace Engineering, Campus Box 7910. Member AIAA Member.

the PCM and fluid due to the particle encapsulating wall, and a homogeneous mixture. Zhang and Faghri [5] numerically tested several of the possible causes and found that the phase-change temperature range caused the majority of the discrepancies. In other numerical work by Ho et al. [7], the discrepancy was attributed to conjugate heat transfer effects within to the copper walled tube used in the experimental work.

For selected materials, the phase-change temperature range and heat rate have been measured using a differential scanning calorimeter (DSC) including eicosane [8,9], technical grade paraffin wax [10], analytical grade octadecane [9], and octacosane [1]. As a simplification of the melting process for phase-change materials a single phase-change temperature has been used in some numerical calculations. The difference between using a single phase-change temperature vs a temperature range in a tubular laminar flow application was calculated and the resulting differences in wall temperature were graphically presented by Zhang and Faghri [5] for eicosane. The measured temperature, heat rate curve specific to eicosane was not used, rather a phase-change temperature range with constant latent heat absorption was found through numerical testing to closely match the experimental data, but the curve was not based on any data other than a melt temperature. The assumption of constant apparent specific heat over the phase-change temperature region has been used in the past as an estimate of the actual process, (Zhang and Faghri [5], Boyer [11], and Hu and Zhang [6]). In addition, several melt models have also been used to solve the heat transfer problem, including Charunyakorn et al. [3] who used a single phase-change temperature and Hu and Zhang [6] who used multiple models including constant, linear, and sinusoidal apparent specific heat over the temperature range.

Ho et al. [7] suggested conjugate heat transfer as a possible source of error. This has previously been studied for single phase fluids and results are available. For example Barozzi and Pagliarini [12] studied laminar flow in a tube with constant heat flux at the outer wall. They found that Peclet number, wall thickness ratio, and thermal conductivity ratio were factors affecting the amount of axial heat transfer within the tube wall. The work of Ho et al. [7] was the only conjugate heat transfer work found for a microPCM suspension.

As a continuation of the above research, numerical modeling was used to calculate the temperature distribution within a microPCM suspension in laminar tube flow with a phase change occurring over a temperature range. Numerical results are presented for several phase-change curves and the results are compared with that of an assumed single phase-change temperature. The current method, using measured DSC results for eicosane from the literature, is used to compare numerical results to the experimental results of Goel et al. [4] Also the effects of conjugate heat transfer on the nondimensional wall temperature are presented for comparison. The numerical code was then used to test the effects of phase-change temperature range vs a single phase-change temperature while varying several dimensionless quantities including Stefan number, phase-change temperature range, and subcooling.

PCM Melting

If the phase change occurs at a single temperature the enthalpy of a microencapsulated PCM particle is a function of temperature with a discontinuity at the phase-change temperature as given by

$$H = \begin{cases} CT & T < T_{\mathrm{sl}} \\ CT_{\mathrm{sl}} + F_{\mathrm{PCM}}\varepsilon L & T = T_{\mathrm{sl}} \\ CT + F_{\mathrm{PCM}}L & T > T_{\mathrm{sl}} \end{cases} \tag{1}$$

However, when phase change occurs over a temperature range the enthalpy of the microencapsulated PCM is given by

$$H = \begin{cases} CT & T < T_l \\ CT + F_{\mathrm{PCM}} \int_{T_s}^{T} f(\tau)\,\mathrm{d}\tau & T_s \le T \le T_l \\ CT + F_{\mathrm{PCM}}L & T > T_l \end{cases} \tag{2}$$

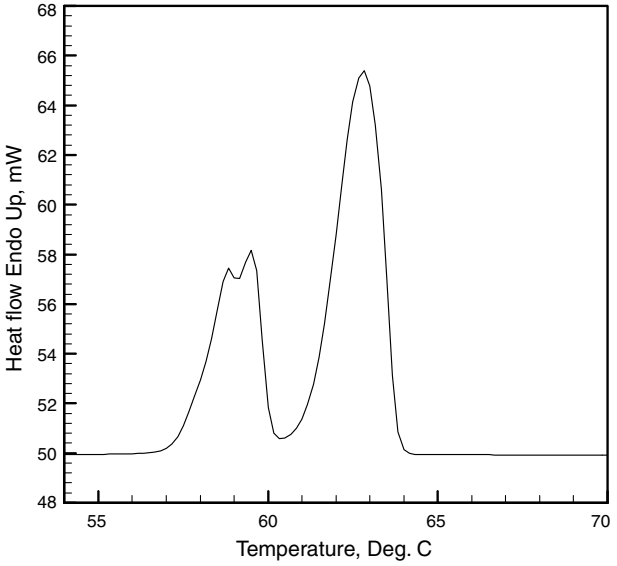

Fig. 1 Typical DSC plot (bulk octacosane) [1].

where $f(T)$ is defined as the specific energy above the sensible energy of the PCM throughout the region of phase change. This is then any energy used for phase transformation, but does not include the energy used to raise the temperature of the PCM. This energy is the energy and may be associated with a solid to liquid phase change or a solid to solid phase change. The latent heat, L, is then found by integrating the specific energy-temperature curve, $f(T)$, over the entire phase-change region,

$$L = \int_{T_s}^{T_l} f(\tau)\,\mathrm{d}\tau \tag{3}$$

A specific energy-temperature curve, $f(T)$, can be found using the results from DSC measurements. Typical results of DSC measurements for octacosane [1] are shown in Fig. 1. The area under the two curves and above the horizontal line represents the latent energy needed to change octacosane from a solid at approximately 55°C to a liquid at 65°C. The total latent heat for octacosane is 259, 100 J/kg. Two peaks are present for this PCM, which represent a solid to solid transition followed by a solid to liquid transition. Using the sample size and temperature change per unit time, the heat flow can be converted to heat per unit mass-temperature, J/kg · C. This temperature dependent quantity includes the specific and latent heats and is referred to as the apparent specific heat where $C_{\mathrm{app}} = f + C$.

Theoretical Development

The governing equation for the application under investigation, a hydrodynamically fully developed laminar flow in a circular tube with constant wall heat flux, is the energy equation

$$(1-c)\left[u\rho_f C_f \frac{\partial T_f}{\partial z}\right] = k_{\mathrm{eff}} \frac{\partial^2 T_f}{\partial z^2} + \frac{1}{r}\frac{\partial}{\partial r}\left(rk_{\mathrm{eff}} \frac{\partial T_f}{\partial r}\right) - S \tag{4}$$

The laminar fluid velocity profile given as

$$u = 2u_m(1 - r^2/R^2) \tag{5}$$

S represents a source term accounting for heat transferred from the carrier fluid to the particles and k_{eff} is the enhanced conductivity due particles in shear flow. An energy balance for the microPCM particles yields the following equation for S in both enthalpy and apparent specific heat form

$$S = cu\rho_p\left(\frac{\mathrm{d}H_p}{\mathrm{d}z}\right) = cu\rho_p\left(C_{\mathrm{app}}\frac{\mathrm{d}T_p}{\mathrm{d}z}\right) = c\frac{3h}{r_p}(T - T_p) \tag{6}$$

The apparent specific heat of a microPCM particle is a function of temperature and is defined using Eq. (2) as

$$C_{p,\text{app}} = \begin{cases} C_p & T < T_l \\ C_p + F_{\text{PCM}} f(T) & T_s \le T \le T_l \\ C_p & T > T_l \end{cases} \tag{7}$$

With a constant heat flux applied at the outer tube radius and a presumed uniform inlet temperature the following boundary conditions apply for the fluid and particle:

$$-k\frac{\partial T_f}{\partial r}\bigg|_{r=R} = q''_R, \qquad \frac{\partial T_f}{\partial r}\bigg|_{r=0} = 0, \qquad T_f|_{z=0} = T_p|_{z=0} = T_{\text{in}}$$
$$H_{\text{PCM}}|_{z=0} = H_{\text{PCM,in}} \tag{8}$$

Equations (4–8) were developed under the following assumptions:

1) The fluid and microPCM particles are moving with the same parabolic velocity distribution for a fully developed laminar flow with a viscosity based on bulk fluid properties.

2) The fluid is an incompressible Newtonian fluid.

3) The material properties are constant.

4) A constant heat flux is applied at the outer tube radius.

5) Particle temperature is at a single temperature throughout, but may be different than the surrounding fluid.

6) Viscous dissipation and axial conduction effects are neglected within the fluid.

7) The particles are monosized and consist of two materials, an encapsulating shell (30% by weight) and a PCM (70% by weight). [4].

8) The particles are evenly distributed microPCM particles throughout the carrier fluid.

9) The flow is axisymmetric.

Defining the following dimensionless parameters

$$r^* = r/R, \qquad r_p^* = R/r_p, \qquad z^* = z/(RPe_b)$$
$$\rho^* = \rho/\rho_b, \qquad C^* = C/C_b, \qquad k^* = k/k_b \tag{9}$$

The governing equations and boundary conditions become

$$(1-c)(1-r^{*2})\rho_f^* C_f^* \frac{\partial \theta_f}{\partial z^*} = \frac{1}{Pe_b^2} k_{\text{eff}}^* \frac{\partial^2 \theta_f}{\partial z^{*2}} + \frac{1}{r^*}\frac{\partial}{\partial r^*}\left(r^* k_{\text{eff}}^* \frac{\partial \theta_f}{\partial r^*}\right) - S^* \tag{10}$$

$$S^* = c(1-r^{*2})\rho_p^* \frac{\partial H_p^*}{\partial z^*} = c(1-r^{*2})\rho_p^* \left[C_{p,\text{app}}^* \frac{\partial \theta_p}{\partial z^*}\right]$$
$$= 3ck_p^* Bi_p r_p^{*2}(\theta - \theta_p) \tag{11}$$

and

$$\frac{\partial \theta_f}{\partial r^*}\bigg|_{r^*=1} = \frac{1}{k_w^*}, \qquad \frac{\partial \theta_f}{\partial r^*}\bigg|_{r^*=0} = 0, \qquad \theta_f|_{z^*=0} = \theta_p|_{z^*=0} = 0$$
$$H_p^*|_{z^*=0} = 0 \tag{12}$$

The source term, S^*, given by Eq. (11) includes two parts; energy due to temperature change and energy due to phase change, and is again shown in enthalpy and apparent specific heat form. An enthalpy form was used by Ho et al. [7], whereas an apparent specific heat form was used by Zhang and Faghri [5]. The current work used the enthalpy form represented by Eq. (11).

The Biot number and effective thermal conductivity of the suspension were presented by Charunyakorn et al. [3] as

$$Bi = \frac{k_{\text{eff}}}{k_p}\frac{2(1-c)}{2-3c^{0.5}+c} \tag{13}$$

$$k_{\text{eff}}/k_b = 1 + BcPe_p^m \tag{14}$$

The bulk fluid conductivity and constants B and m are defined in [3] and the particle Peclet number is also given in [3] as

$$Pe_p = e(2r_p)^2/\alpha_f \tag{15}$$

The effects of particle wall thickness were included by modifying the Biot number to use an overall heat transfer coefficient, U, instead of the heat transfer coefficient, h. For spherical particles the overall heat transfer coefficient is

$$U = \frac{hk_{p,w}}{k_{p,w} + h(r_2^2/r_1 - r_2)} \tag{16}$$

An alternate Biot number was found using Eq. (16), which includes the wall resistance

$$Bi^+ = \frac{Ur_p}{k_p} = Bi\frac{k_{p,w}/k_p}{k_{p,w}/k_p + Bi(r_p/r_{\text{PCM}} - 1.0)} \tag{17}$$

The governing equations for the axis-symmetric tube wall are the steady state heat conduction equation along with the following boundary conditions: constant outer wall heat flux, a heat flux match at the fluid-wall interface, and adiabatic end conditions. The adiabatic end conditions were chosen to represent the experimental setup of Goel et al. [4], which used plastic inlet and outlet isolation sections (the thermal conductivity of plastics is generally 3 orders of magnitude lower than the copper tube wall used in the test section). The governing equation and boundary conditions for the tube wall in dimensionless form are

$$\frac{1}{Pe^2}\frac{\partial^2 \theta_w}{\partial z^{*2}} + \frac{1}{r^*}\frac{\partial^2 \theta_w}{\partial r^{*2}} = 0 \tag{18}$$

$$-\frac{\partial \theta_w}{\partial r^*}\bigg|_{r^*=1+\Delta} = \frac{k_b}{k_w(1+\Delta)} \qquad \frac{\partial \theta_w}{\partial r^*}\bigg|_{r^*=1} = \frac{k_b}{k_w}\frac{Nu_z}{2}(\theta_w - \theta_m)$$
$$\frac{\partial \theta_w}{\partial z^*}\bigg|_{z^*=0} = \frac{\partial \theta_w}{\partial z^*}\bigg|_{z^*=Z^*} = 0 \tag{19}$$

The Nusselt number in Eq. (19) was used in the numerical solution to transfer thermal information from the tube wall to the fluid in an iterative fashion. The local Nusselt number was based on an arithmetic average slurry temperature at an axial location as shown in Eq. (20). Note that this average temperature is different than a "mixed cup" temperature due to the latent energy storage of the PCM.

$$Nu_z = \frac{2q''_{R,z}/q''_R}{(\theta_{w,z} - \theta_{m,z})} \tag{20}$$

where $q''_R = q''_{R+\Delta}(1+\Delta/R)$is the constant heat flux at the tube inner wall and $q''_{R,z}$is the local heat flux at an axial position. These quantities are equal when there is no tube wall.

Modeling

The quadratic upstream interpolation for convective kinematics (QUICK) scheme [13] was used to model Eq. (10) and calculate the dimensionless temperature of the fluid, whereas a second order backwards method was used to model the energy transferred from the fluid to the microPCM particles. Grid independence was checked by successively reducing grid size and comparing the converged solutions. The final grid size used was 380 radial steps and 1140–2280 axial steps (depending on the tube length), both evenly spaced. Verification of the numerical model included overall energy balances, comparison to previous numerical results of conjugate heat transfer using a single phase heat transfer fluid [12], and also comparison to the experimental results of Goel et al. [4], which used eicosane as the PCM and water as the carrier fluid. The single phase conjugate heat transfer comparison is shown in Fig. 2, whereas the experimental results comparison is discussed in the experimental comparison section. A minimum of 99.9% of the overall energy was conserved for all cases.

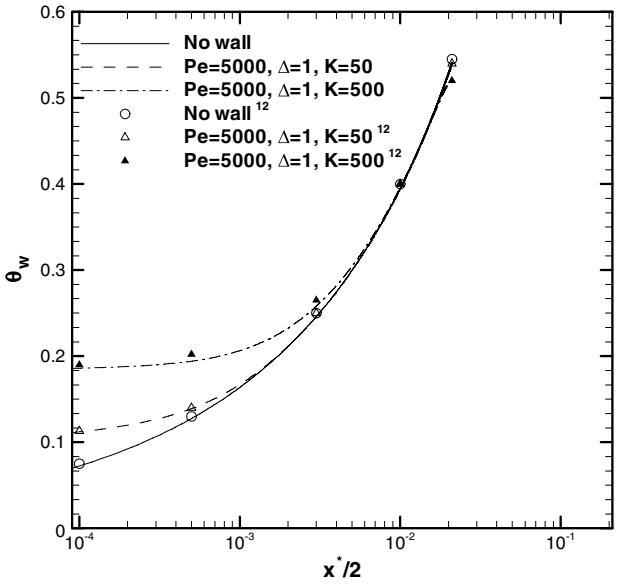

Fig. 2 Single phase fluid tube wall temperature comparison: previous results from the literature to results of the current work.

Latent Heat and Physical Properties

Zhang and Faghri [5] assumed the latent heat absorption to be constant over a temperature range of 34.4 to 36.7°C, whereas the present work uses the DSC measurements by Montenegro and Landfester [8] to characterize the latent heat absorbed by the eicosane throughout the phase-change temperature range. A curve fit of this experimentally determined heat flow curve was made and is presented in Fig. 3a. The curve fit represents a latent heat of 233,000 J/kg and is a combination of a parabolic and Gaussian curves given by Eq. (21). The melt temperature range is 34 to 44°C with a single peak occurring at $T_{\max} = 40$°C where $\sigma_{\text{sl}} = 0.9$°C and $T_s = 34$°C.

$$f = \begin{cases} \frac{0.44L}{\sqrt{2\pi\sigma_{\text{sl}}^2}}\left(1 - \frac{(T-T_{\max})^2}{(T_s-T_{\max})^2}\right) & T_s < T < T_{\max} \\ \frac{0.44L}{\sqrt{2\pi\sigma_{\text{sl}}^2}}\exp\left(-\frac{(T-T_{\max})^2}{\sqrt{2\sigma_{\text{sl}}^2}}\right) & T_{\max} \le T < T_l \end{cases} \tag{21}$$

In dimensionless form over the two temperature ranges Eq. (21) becomes

$$f^* = \begin{cases} \frac{0.44}{c\rho_p^* \text{Ste}\sqrt{2\pi\sigma_{\text{sl}}^{*2}}}\left(1 - \frac{(\theta-\theta_{\max})^2}{(\theta_s-\theta_{\max})^2}\right) \\ \frac{0.44}{c\rho_p^* \text{Ste}\sqrt{2\pi\sigma_{\text{sl}}^{*2}}}\exp\left(-\frac{(\theta-\theta_{\max})^2}{\sqrt{2\sigma_{\text{sl}}^{*2}}}\right) \end{cases} \tag{22}$$

By comparison constant absorption of heat over a temperature range (box method) is given by

$$f = L/(T_s - T_l) \tag{23}$$

In dimensionless form this becomes

$$f^* = 1/(c\rho_p^* Ste(\theta_l - \theta_s)) \tag{24}$$

Integration of Eq. (21) will yield the latent heat as a function of temperature for eicosane throughout the phase-change region. Figure 3 includes a plot of Eqs. (21) and (23) and the latent heat as a function of temperature. By comparison the single temperature phase change would show a discontinuity in latent heat at the phase-change temperature, whereas a constant absorption (i.e., box) is a linearly increasing latent heat over the temperature range whose slope will increase as the phase-change temperature range decreases. The constant absorption of heat over a temperature range (box method) has been a common assumption of much numerical work [5,6,11]. Thermal conductivity, specific heat, viscosity, and density of the slurry were those reported by Goel et al. [4]. In addition, the density and thermal conductivity of the copper tube wall were set to 8933 kg/m^3 and 401 W/(m · K) [14], respectively.

Particle Wall Resistance

The added resistance of the particle wall was investigated by including the resistance, via Eq. (17), and comparing this with the case where the particle wall resistance was neglected. Figure 4a presents the axial tube wall temperature with and without particle wall resistance for two cases of phase change; phase change at a single temperature ($\theta_{\text{sl}} = 0$) and phase change over a temperature range using the curve fit data. When the phase-change temperature range was zero there was a slight but noticeable difference in tube wall temperature between neglecting and including the particle wall resistance, but when using a phase-change temperature range the difference was nearly zero (see Fig. 4a). The particle wall resistance has been included in all subsequent calculations.

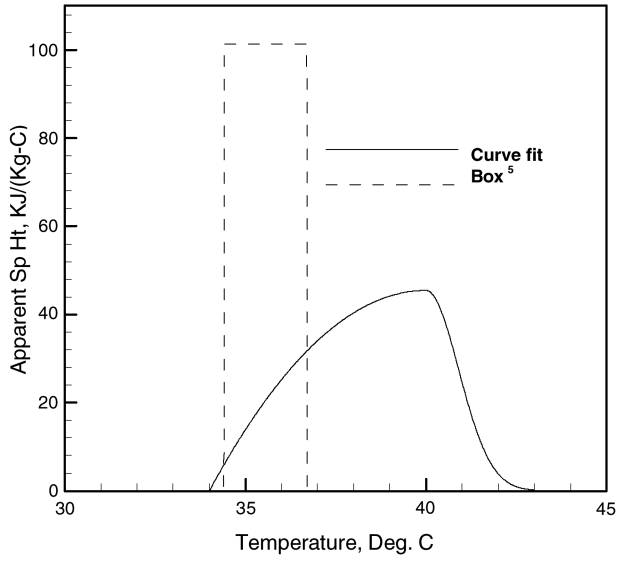

a)

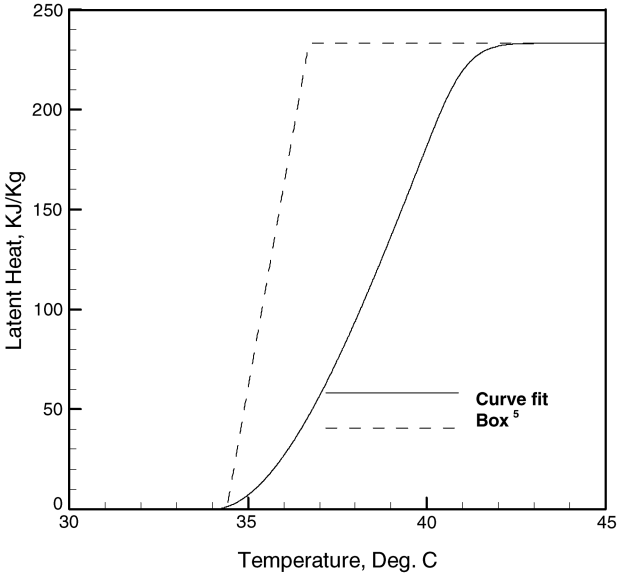

b)

Fig. 3 Eicosane phase change, a) apparent specific heat and b) latent heat.

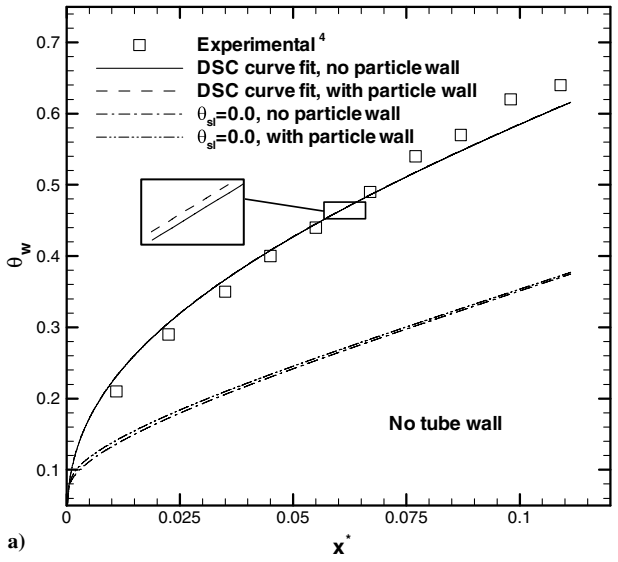

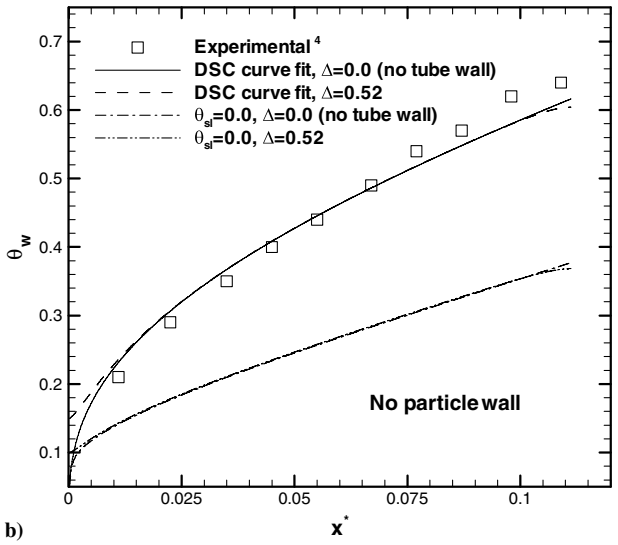

Fig. 4 Experimental comparison, a) particle wall effects and b) tube wall effects.

Comparison

Numerical results, Figs. 4a and 4b, using a single phase-change temperature of 36.7°C resulted in dimensionless axial wall temperatures much lower than those of the experimental work of Goel et al. [4], but are consistent with the numerical results of Charunyakorn et al. [3] and Zhang and Faghri [5]. Numerical results of Zhang and Faghri [5] also used a dimensionless phase-change temperature range of $\theta_{sl} = \theta_l - \theta_s = 0.4$ ranging from $\theta_s = -0.33$ to $\theta_l = 0.07$, which was found to closely match the experimental results of Goel et al. [4] for a 10% particle concentration of microencapsulated eicosane at a Reynolds number of 200 and a Stefan number of 1.0. This phase-change temperature range had a constant apparent specific heat with 17.5% of the total latent heat above the dimensionless inlet temperature. This range, however, had no physical basis other than the tube wall temperature results matched the experimental data. The dimensionless phase-change temperature range for the DSC data curve fit was $\theta_s = -1.58$ to $\theta_l = 2.98$, with 86% of the total latent heat above the inlet temperature. The DSC curve fit, Eq. (22), results are presented in Fig. 4. The tube wall temperature matched the experimental data of Goel et al. [4] when representing the phase change found by a DSC with a curve fit.

For each phase-change model, the tube wall conjugate effects were tested and are presented in Fig. 4b. The difference of including the tube wall for each case was found to be minimal with the largest discrepancy at the inlet and outlet of the tube. These results are consistent with that of a single phase fluid as found by Barozzi and Pagliarini [12]. The difference in wall temperature using a single melt temperature vs a melt range was found to be the major cause of discrepancy. This agrees with the finding of Zhang and Faghri [5] and differs from the findings of Ho et al. [7] in which the tube wall effects were identified as the source of discrepancy.

Results and Discussion

Baseline Case

To study the effects that the phase-change temperature range has on the outer tube wall temperature, the following parameters for a general baseline case were used (the particle properties, tube wall thickness, and concentration were those used by Goel et al. [4]):

$$Re_b = 200, \quad r_p^* = 15.7, \quad \theta_m = 0.07, \quad Ste = 1$$
$$Pr_b = 10, \quad \rho^* = 1.0, \quad C_f^* = 1.0, \quad C_p^* = 1.0$$
$$\Delta = 0.5, \quad K = 500.0 \tag{25}$$

The density ratios were set to unity to simulate a neutrally buoyant particle. The function, $f(T)$, was taken to be constant over the melting temperature range and was set to a level for each phase-change temperature range to represent an equal amount of latent heat over the phase change. The effectiveness of estimating the energy absorbed during phase change as a constant has been the subject of several publications including Hu and Zhang [6] and Bart and van der Laag [15]. In addition, a method of choosing a width and anchor point for a particular PCM was discussed by Bart and van der Laag [15], however, to represent a general phase-change material, the box method with the phase-change region centered at the melt temperature was used in this work.

Varying Phase-Change Temperature Range

Numerical results for the baseline conditions are shown in Fig. 5a and 5b with three dimensionless phase-change temperature ranges being used, $\theta_{sl} = 1.0$, 0.5, and 0.0 (phase change at a single temperature). Using Eq. (24), $f^* = 10.0$, 20.0, and ∞. The values of θ_{sl} show a progression of temperature curves from a wide temperature range to a single phase-change temperature. Both the dimensionless tube wall, Fig. 5a, and fluid temperatures across the radius at the exit, Fig. 5b, are presented. Because the range is centered on the melt temperature, $\theta = 0.07$, the wider temperature ranges have some portion of the latent heat below the inlet temperature and therefore were not available during the heating process, specifically 43% and 18% for $\theta_{sl} = 1.0$ and 0.5, respectively. As the temperature range becomes smaller and more of the latent heat was above the inlet temperature, the dimensionless tube wall temperature becomes lower over the majority of the tube length, Fig. 5a.

At the inlet the no tube wall case with a melt range of $\theta_{sl} = 0.0$ was initially the highest temperature until shortly after the tube wall temperature reaches the melt temperature, which is characterized by a change in the slope of the axial tube wall temperature. This is due to inlet subcooling, where the PCM has not yet reached the phase-change temperature. When tube wall effects were included, this phenomenon was eliminated, due to axial heat transfer. After an inlet region, extending to nearly $x^* = 0.01$, there was virtually no difference between the tube wall temperatures for the inner tube wall, the outer tube wall, and the no tube wall case for each phase-change temperature range as seen in Fig. 5a. As such, the tube wall effects will be included and the outside tube wall temperature will be presented for the remainder of the analysis.

The radial variation in dimensionless fluid temperature at the tube exit was also plotted, Fig. 5b, and shows the progression from a wide temperature range to that of a phase change at a single temperature. The particle and fluid temperature are nearly the same when the wider phase-change range is used. In contrast, during a phase change at a single temperature there is a larger temperature difference between the fluid and particles when the particles are at the phase-change

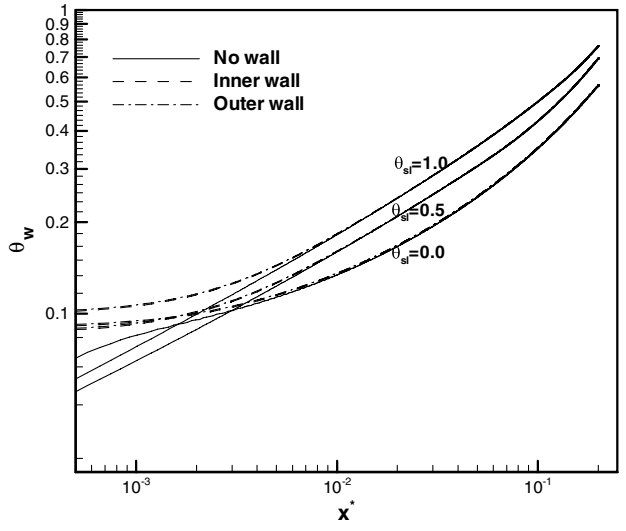

a)

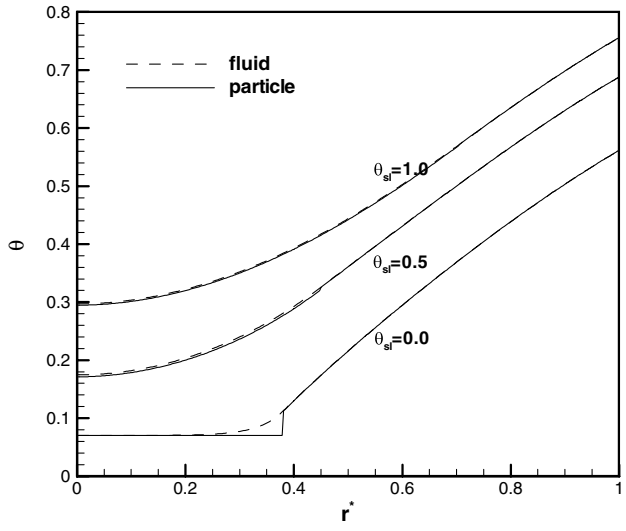

b)

Fig. 5 Baseline comparison, a) axial wall temperature and b) radial exit temperature.

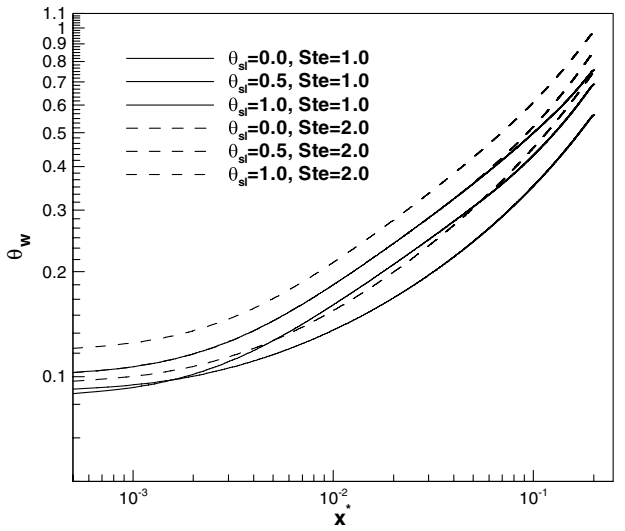

a)

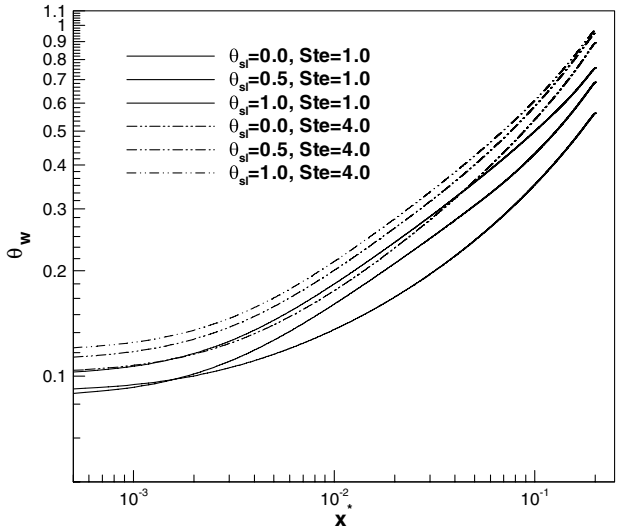

b)

Fig. 6 Wall temperature at varying Stefan numbers, a) *Ste* = 1.0 and 2.0 and b) *Ste* = 1.0 and 4.0.

temperature. The particles remain at a single temperature, $\theta = 0.07$, during the phase-change process and abruptly increases temperature to the fluid temperature when phase change has completed. A larger rate of heat transfer from the fluid to the particle is expected here due to the larger particle to fluid temperature difference. From this point forward, comparisons will be made using three phase-change temperature ranges: $\theta_{sl} = 1.0$, 0.5, and 0.0.

Stefan Number

Two larger Stefan numbers, $Ste = 2.0$ and 4.0 with $f^* = 5.0$ and 10.0 at $\theta_{sl} = 0.5$ and $f^* = 2.5$ and 5.0 at $\theta_{sl} = 1.0$, were also investigated and the results are presented in Fig. 6. An increase in Stefan number could be due to a higher wall heat flux, a PCM with a lower latent heat, or a lower concentration, as each of these will cause an increase in the Stefan number. As the Stefan number was increased, the dimensionless wall temperature increased as should be expected from Eqs. (22) and (24), which shows as the Stefan number approaches infinity the specific energy function $f(T)$ approaches zero. This in turn causes the apparent specific heat to approach the actual specific heat of the particle. In this limit, the fluid temperatures will be the same as a slurry with no phase change. The lower phase-change temperature ranges of 0.5 and 0.0 had the lowest wall temperatures for both of the higher Stefan numbers, as was the case for the baseline. When the Stefan number was increased to four, the difference between the three phase-change ranges became less. This is consistent with the infinite limit of the Stefan number discussed above.

Inlet Subcooling

Two inlet dimensionless subcooling temperatures, $\theta_{sb} = 0.25$ and 0.5, were investigated and the results presented in Fig. 7. As the inlet subcooling was increased the tube wall temperature of the zero phase-change range $\theta_{sl} = 0.0$ was higher than these for the wider phase-change ranges. When the fluid temperature was increased to the melt temperature there was a decrease in the slope of the single temperature phase-change tube wall temperature. The increased subcooling caused a longer inlet region giving a higer tube wall temperature, when $\theta_{sl} = 0.0$. For the larger phase-change range case the resulting tube wall temperatures were the same for most of the length of the tube until near the exit when the added available latent heat caused the tube wall temperature to be below the lower subcooling values.

Conclusions

A method to numerically predict fluid temperature when using a microPCM slurry in laminar flow was used to compare published

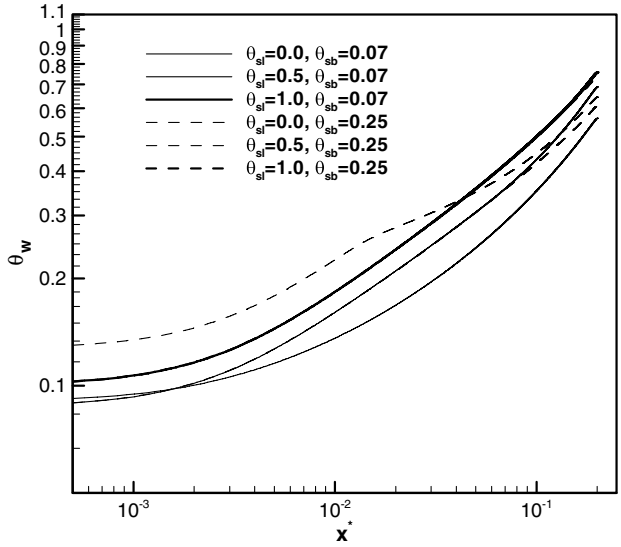

a)

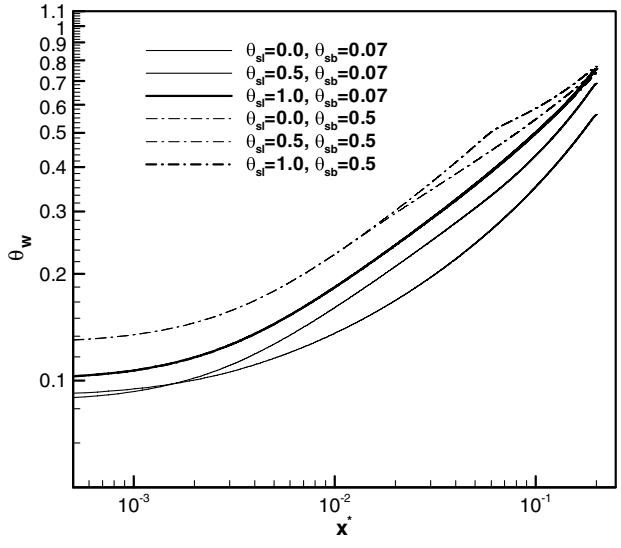

b)

Fig. 7 Wall temperature at varying subcooling, a) $\theta_{sb} = 0.07$ and 0.25 and b) $\theta_{sb} = 0.07$ and 0.5.

experimental and numerical results of previous work. The insulating effect of the encapsulating material surrounding the phase-change material was investigated and found to minimally affect the tube wall temperature. The effect was most noticeable when the phase-change temperature range was at or near zero. Axial tube wall conduction was also investigated with noticeable differences in wall temperature at the inlet and minimal difference throughout the majority of the tube length; these findings are similar to results of single phase fluid flow. The phase-change temperature range was found to have a significant effect on the wall temperature of the tube and can cause large differences between numerical and experimental results. For a general PCM, using a constant heat absorption rate over several phase-change temperature ranges, the effect of the range was mainly found to be due to the amount of latent heat which was available above the inlet temperature. The wider phase-change temperature ranges had less available latent heat when the subcooling was small.

References

[1] Jackson, W. B., Gould, R. D., and Mulligan, J. C., "Performance of an Octacosane Based MicroPCM Fluid for Cooling EV Electronics," AIAA Paper 2002-3226, 24–26 June 2002.

[2] Hao, Y. L., and Tao, Y. X., "A Numerical Model for Phase-Change Suspension Flow in Microchannels," *Numerical Heat Transfer, Part A*, Vol. 46, No. 1, 2004, pp. 55–77. doi:10.1080/10407780490457545

[3] Charunyakorn, P., Sengupta, S., and Roy, S. K., "Forced Convection Heat Transfer in Microencapsulated Phase Change Material Slurries: Flow in Circular Ducts," *International Journal of Heat and Mass Transfer*, Vol. 34, No. 3, 1991, pp. 819–835. doi:10.1016/0017-9310(91)90128-2

[4] Goel, M., Roy, S. K., and Sengupta, S., "Laminar Forced Convection Heat Transfer in Microencapsulated Phase Change Material Suspensions," *International Journal of Heat and Mass Transfer*, Vol. 37, No. 4, 1994, pp. 593–604. doi:10.1016/0017-9310(94)90131-7

[5] Zhang, Y., and Faghri, A., "Analysis of Forced Convection Heat Transfer in Microencapsulated Phase Change Material Suspensions," *Journal of Thermophysics and Heat Transfer*, Vol. 9, No. 4, 1995, pp. 727–732.

[6] Hu, X., and Zhang, Y., "Novel Insight and Numerical Analysis of Convective Heat Transfer Enhancement with Microencapsulated Phase Change Material Slurries: Laminar Flow in a Circular Tube with Constant Heat Flux," *International Journal of Heat and Mass Transfer*, Vol. 45, No. 15, 2002, pp. 3163–3172. doi:10.1016/S0017-9310(02)00034-0

[7] Ho, C. J., Lin, J. F., and Chiu, S. Y., "Heat Transfer of Solid-Liquid Phase-Change Material Suspensions in Circular Pipes: Effects of Wall Conduction," *Numerical Heat Transfer, Part A*, Vol. 45, No. 2, 2004, pp. 171–190.

[8] Montenegro, R., and Landfester, K., "Metastable and Stable Morphologies During Crystallization of Alkanes in Miniemulsion Droplets," *Langmuir*, Vol. 19, No. 15, 2003, pp. 5996–6003. doi:10.1021/la027019v

[9] Lan, X., Tan, Z., Zou, G., Sun, L., and Zhang, T., "Microencapsulation of n-Eicosane as Energy Storage Material," *Chinese Journal of Chemistry*, Vol. 22, No. 5, 2004, pp. 411–414.

[10] Gibbs, B. M., and Hasnain, S. M., "DSC Study of Technical Grade Phase Change Heat Storage Materials for Solar Heating Applications," *Solar Engineering*, Vol. 2, 19–24 March 1995, pp. 1053–1062 (The 1995 ASME/JSME/JSES International Solar Energy Conference).

[11] Boyer, D., "A Numerical Model of a Suspension Containing Microencapsulated Phase Change Material Flowing Through a Tube Using the Enthalpy Method," M.S. Thesis, North Carolina State University, Raleigh, NC, 1997.

[12] Barozzi, G. S., and Pagliarini, G., "A Method to Solve Conjugate Heat Transfer Problems: The Case of Fully Developed Laminar Flow in a Pipe," *Journal of Heat Transfer*, Vol. 107, Feb. 1985, pp. 77–83.

[13] Leonard, B. P., "A Stable and Accurate Convective Modeling Procedure Base on Quadratic Upstream Interpolation," *Computer Methods in Applied Mechanics and Engineering*, Vol. 19, No. 1, 1979, pp. 59–98. doi:10.1016/0045-7825(79)90034-3

[14] Incropera, F. P., and DeWitt, D. P., *Fundamentals of Heat and Mass Transfer*, 5th ed., Wiley, New York, 2002, p. 905.

[15] Bart, G. C. J., and van der Laag, P. C., "Modeling of Arbitrary-Shaped Specific and Latent Heat Curves in Phase-Change Storage Simulation Routines," *Journal of Solar Engineering*, Vol. 112, Feb. 1990, pp. 29–33.